Accuracy of sub-pixel interpolation in PIV and PTV image processing

H. Nobach

March 15, 2004

This report investigates the accuracy of the velocity estimation using the Particle Image Velocimetry (PIV) or Particle Tracking Velocimetry (PTV) and introduces possible improvements to PIV yielding more accurate and more robust velocity estimates under given conditions and extending the application range of this technique.

Contents

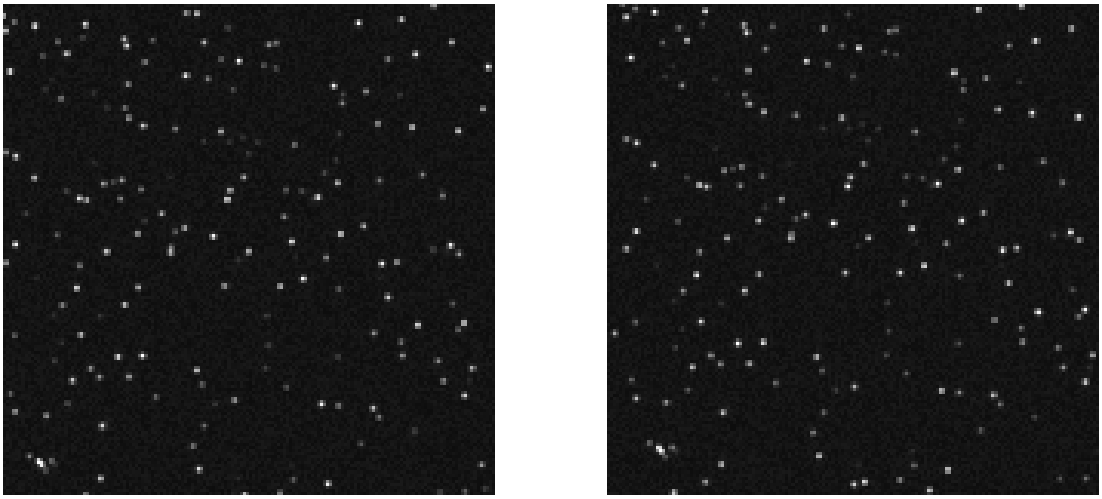

Figure 1: PIV/PTV image pair

1 Introduction

Both techniques, the PIV and the PTV are analysing methods for image pairs taken in a seeded flow field with known temporal distance (figure 1). The distance between the particle positions in the two images yields the local velocity information. While the PTV method directly traces single particles, the PIV uses the cross-correlation function to derive statistically the motion (figure 2). Therefore, the possible accuracy of the PTV algorithm is given by the accuracy of the detection of particle positions, whereas the PIV method is limited by the accuracy of locating the correlation peak.

In both cases a transform from image co-ordinates into orthogonal real-world co-ordinates can be necessary, e.g. for stereoscopic or any other non-orthogonal imaging. This requires a resampling of the images, as also the window deformation technique [Huang et al. (1993); Scarano (2002)] does. Since deviations of the interpolated intensity distribution directly influence the velocity estimate, this is also a critical procedure, which should guarantee a minimum loss of information.

As no camera objective is ideal, the real particle images on the image plane are distorted due to the limited spatial bandwidth of the camera objective and due to aberrations. These two effects are combined in the point-spread function of the camera objective [Ronneberger et al. (1998)]. The following section investigates the accuracy of estimating the position of particles using a simplified model. The continuous intensity function is given by a Gaussian or by an Airy function, which is either sampled at the pixel center positions or integrated over the pixel area.

In section 3 the loss of information due to an interpolation is shown using different interpolation methods.

Section 4 investigates the possible accuracy of displacement estimation between two images using the cross-correlation function between images with single par-

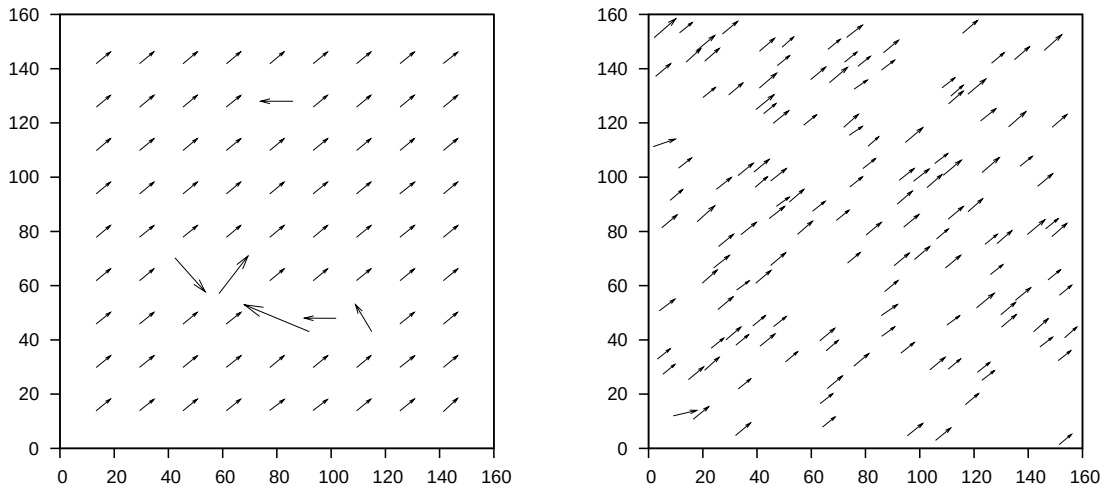

Figure 2: PIV (a) and PTV (b) results

ticle images or more particle images. In the latter case also the possibility of truncated particle images at the borders of interrogation areas is recognized.

In all cases, the influence of a background gray level and noise has been investigated and the most accurate algorithms are given.

First, all these investigations are done with one-dimensional signals. In section 5 the algorithms are adapted to two-dimensional images and in section 6 they are applied to simulated and real data.

Section 7 concludes with an outlook.

2 Estimation of particle positions from the image

The accurate estimation of the particle position from the obtained images is essential for the PTV analysis. In this section several routines are investigated, which derive the particle sub-pixel position from the discrete intensity field. At this point no image interpolation is used. The influence of the interpolation routine is shown in the next section.

2.1 Gaussian particle image

The most simple model of the imaging process of a small particle is the Gaussian function of intensity, which is regularly sampled by the camera [Willert and Gharib (1991)]. For simplification, only a one-dimensional function is used. Figure 3 shows a Gaussian function. The width is 2 pxl, which is defined by the e^{-2} of the maximum value.

A widely used method to derive the sub-pixel position of the maximum is to fit a Gaussian function to the samples and to derive the maximum position of

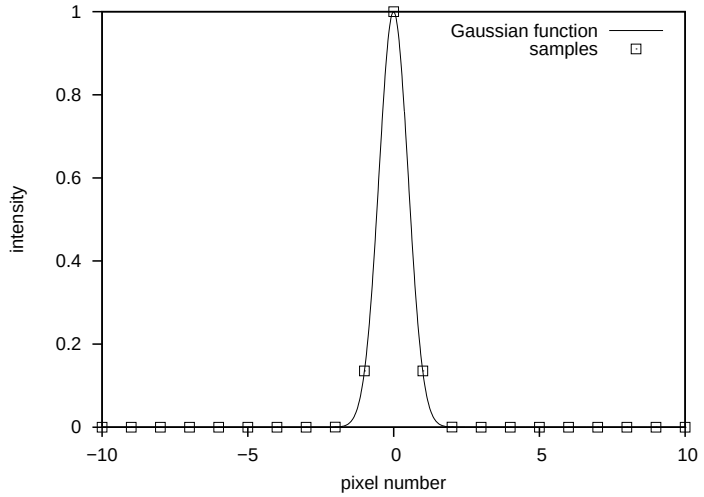

Figure 3: Gaussian function and the obtained samples

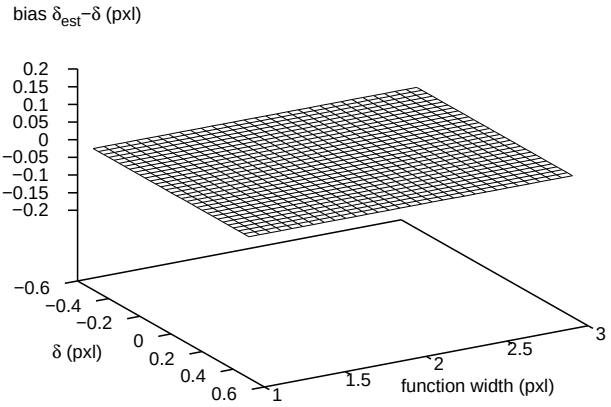

Figure 4: Sub-pixel position bias for Gaussian intensity functions

the interpolation function. Since the logarithm of a Gaussian function yields a second order polynomial, the sub-pixel position δ of the interpolants maximum can be derived as

$$\delta = \frac{Y_{I-1} - Y_{I+1}}{2\left(Y_{I+1} - 2Y_I + Y_{I-1}\right)} \tag{1}$$

relatively to the index I of the maximum sample, where Y_i is the logarithm of the functions value y_i.

This interpolation method works exactly for a wide range of Gaussian functions. In figure 4 the estimated deviation of the sub-pixel estimation is shown as a function of the width and the exact sub-pixel position. In this ideal case no significant bias can be seen.

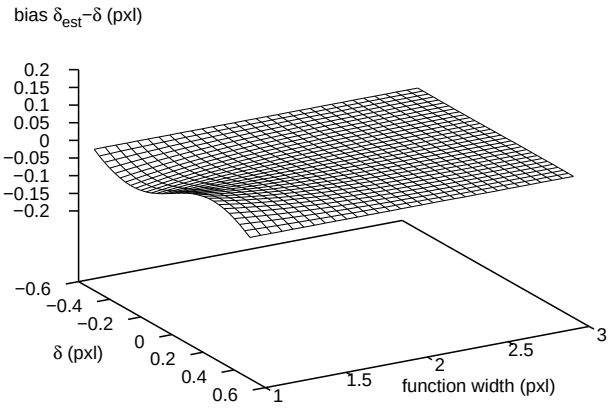

Figure 5: Sub-pixel position bias for Gaussian intensity functions using the pixel integration

2.2 Gaussian particle image with pixel integration

In real world the pixel intensity function of a photo camera is not given as a sampling of the spatial intensity field. The intensity value of a specific image pixel is given as the integral of the spatial intensity field over the pixels area. Details about the imaging model can be found in Ronneberger et al. (1998). The model used here is more simple. A continuous Gaussian intensity function or an Airy function (next section) is integrated over a square pixel area of the size $1\,\text{pxl} \times 1\,\text{pxl}$.

In figure 5 a Gaussian function has been partwise integrated yielding the intensity values. For this function equation (1) has been used to derive the sub-pixel position.

For very thin Gaussian function a bias of the sub-pixel position estimation can be seen. However, for widths larger than 2 pxl this bias is smaller than 0.01 pxl.

2.3 Airy particle image with pixel integration

The particle image does not comply with the Gaussian function model. Due to the limited optical resolution of the imaging system for the best focus, the imaging function becomes an Airy disc.

Here only the one-dimensional case has been investigated. Again this function has been integrated partwise to yield a realistic intensity function and equation (1) has been used to derive the sub-pixel position.

Figure 6 shows the bias of the sub-pixel position estimation as a function of the width of the Airy function and the exact position. For very thin functions a bias of the sub-pixel position estimation can be seen. This bias does not much exceed the bias for the Gaussian function. This is due to the pixel area integration, which smooths the Airy function towards a Gaussian function. However, for widths larger than 2 pxl this bias is smaller than 0.02 pxl.

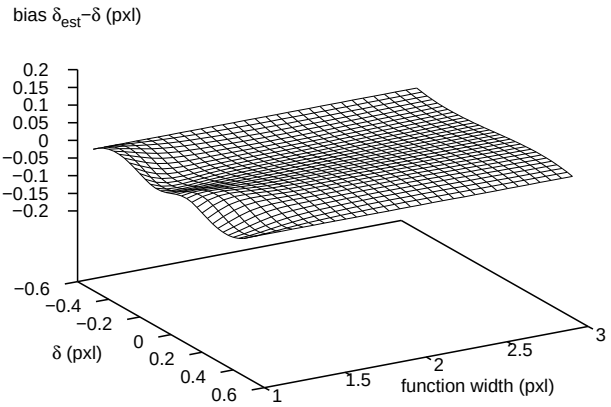

Figure 6: Sub-pixel position bias for an Airy intensity functions using the pixel integration

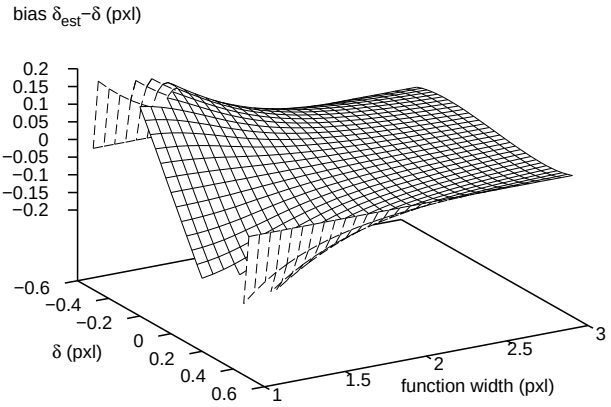

Figure 7: Sub-pixel position bias for Gaussian intensity functions with offset

2.4 Offset of gray values

Due to the logarithm, the equation (1) is sensitive to the offset of the gray values. Therefore, the background of the PIV-image must be subtracted before the sub-pixel position estimation can be done. The estimation of the background intensity is influenced at least by local fluctuations over the image and image noise. A further influence can occur if the estimation of the background intensity is done without masking the high intensity of the particle images.

To separate the influence of an offset, the Gaussian function has been sampled as in figure 4 and a constant value of 0.1 has been added and, again, equation (1) has been used to derive the sub-pixel position. The results are shown in figure 7. A significant deviation can be seen, which decreases for wider functions. For a width of 2 pxl this bias can reach 0.06 pxl and for a width of 3 pxl still more than 0.01 pxl.

To reduce the influence of the gray value an extended Gaussian model can be

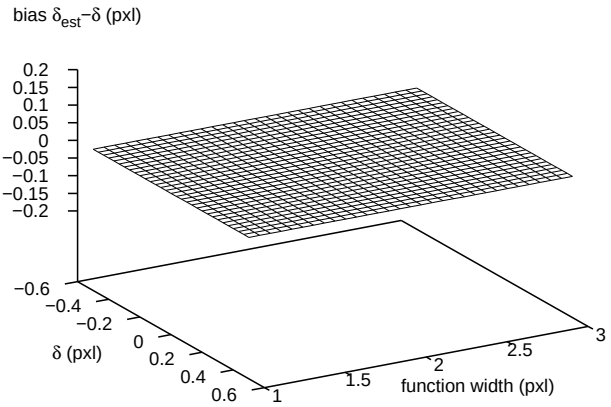

Figure 8: Sub-pixel position bias for Gaussian intensity functions with offset using the 4-parameter Gaussian model

used which includes the offset as an additional parameter

$$y(x) = a \exp\left[-b(x-c)^2\right] + d \tag{2}$$

This model function is fit to the 5 points around the maximum. The parameters are estimated using an iterative optimization routine, which minimizes the following error at the location of the maximum, I.

$$e = \sum_{i=I-2}^{I+2} \left[y_i - \left(a \exp\left[-b(i-c)^2\right] + d\right)\right]^2 \rightarrow \min \tag{3}$$

The result is shown in figure 8, where the 4-parameter Gaussian model has been fit to a sampled Gaussian function with an offset. The remaining bias is negligible.

3 Estimation of particle positions from the image after interpolation

Often in the PIV analysis, the image values are required at sub-pixel positions, e.g. the transformation of the coordinates of oblique images into real cartesian coordinates or the window deformation technique [Huang et al. (1993); Scarano (2002)]. Therefore, the image is interpolated using an interpolation function and resampled at new positions.

The bias of the sub-pixel position estimation after the interpolation and resampling with a linear function is shown in figure 9 as a function of the correct sub-pixel position δ and the distance of the resampling points to the original sampling locations δ_{res}. With a used width of the Gaussian function of 2.5 pxl the maximum bias is about 0.11 pxl and significantly exceeds the bias sources

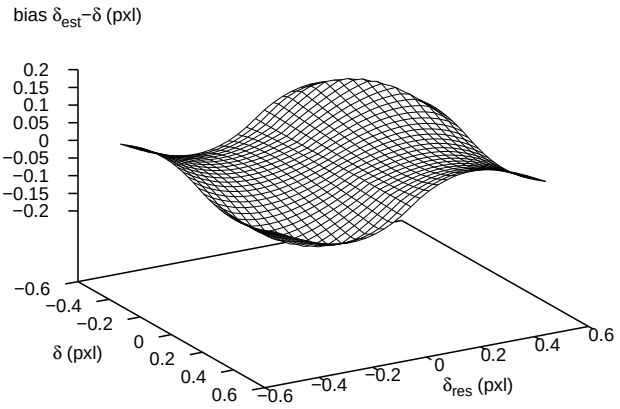

Figure 9: Sub-pixel position bias for Gaussian intensity functions with a linear interpolation

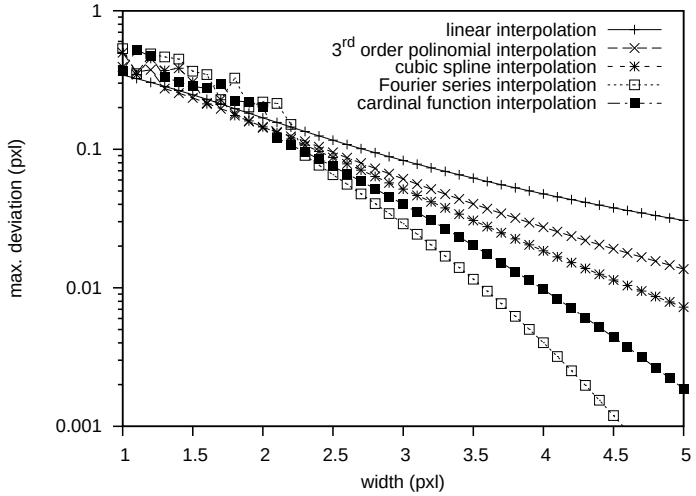

Figure 10: Sub-pixel position bias for Gaussian intensity functions for several interpolation methods

investigated above. To avoid loss of information in the resampling process, better interpolation methods should be used than the linear interpolation, which is widely used due to its simplicity and robustness.

The image re-sampling is a crucial step for the appropriate reconstruction of the image signal as has been shown by Pratt (1978). In Scarano (2002) several interpolation schemes have been mentioned. Higher-order polynomial functions are given as superior to the linear interpolation. Therefore, a 3rd order polynomial interpolation, a cubic spline interpolation with 20 points, a Fourier series interpolation and a cardinal function interpolation [Hall (1979)] with a Hamming window to reduce the abruptness of the truncated ends of the sinc function [Niblack (1986)] have been investigated.

In figure 10 the maximum bias of the sub-pixel position estimation is shown as

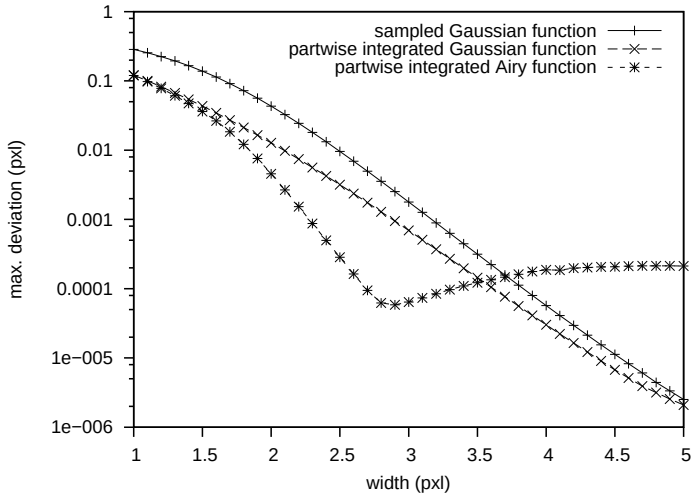

Figure 11: Sub-pixel position bias for the Gaussian model interpolation for several intensity functions

a function of the width of the Gaussian function for several interpolation schemes. Indeed, the higher-order interpolation schemes are better than the simple linear interpolation. However, the remaining bias cannot be neglected.

As mentioned in Scarano (2002) the PIV signal spectrum has a major component in the high-frequency part, at least for diameters less than 3 pxl. The Nyquist criterion is not fulfilled and the PIV image is under-sampled. Therefore, all interpolation schemes based on the sampled function only fail. Even the cardinal function has a significant bias up to a particle image diameter of 4 pxl. This result is different from those in Roesgen (2003), which can be explained as a result of using larger particle images there.

More accurate results can be achieved using an optimized interpolation filter, recognizing the signal character and the signal model used for the estimation of the sub-pixel location. For high robustness a 11-point Gaussian filter is used with the coefficients

$$c_i(x) = \exp\left[-b(x-i)^2\right] \quad \text{for } i = X-5 \ldots X+5 \tag{4}$$

where X is the rounded integer value of the resample positions $x = j + \delta_{res}$. The parameter b has been found to be optimal at $b = 0.4$. Note that this value is optimal only for signals without noise, which have been investigated here. For noisy signals this value must be chosen larger (section 4.5).

Figure 11 shows the results obtained for the Gaussian filter interpolation using several intensity function. This interpolation scheme is clearly superior to the methods above. For a width of 2.5 pxl a systematic error of less than 0.01 pxl remains for the Gaussian intensity function. For the partwise integrated Gaussian intensity function and the partwise integrated Airy function the results are even better. For the latter one and peaks of ≥ 2.2 pxl width a systematic error of

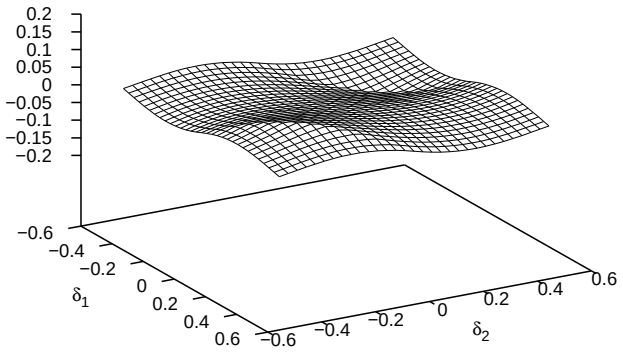

Figure 12: Sub-pixel displacement bias for the Gaussian model interpolation applied to a sampled Gaussian intensity function

less than 10^{-3} pxl, and for peaks with a width between ≥ 2.5 pxl and ≥ 4.0 pxl a systematic error of less than 10^{-4} pxl remains.

The results of the Gaussian interpolation comply with Roesgen (2003), whereas the results using the sinc interpolation scheme do not. Obviously, the size of the particle image has been chosen there large enough to fulfil the Nyquist criterion sufficiently. On the other hand, the usual size of particle images is in the range of 2 or 3 pxl, where a significant bias remains for the sinc interpolation scheme, while the Gaussian interpolation scheme even in this range yields excellent results.

4 Estimation of displacement between two images

In this section the displacement between two images with single peaks is investigated. For these principal investigations, again only one-dimensional signals are used.

4.1 Estimation from single peaks without image interpolation

In PIV analysis the displacement of a particle ensemble between two images is estimated using the cross correlation function of the two images. The result is given in image coordinates (pixel). A transformation of the image coordinates into real length coordinates before the cross correlation requires an image interpolation and resampling, which is not investigated here.

To quantify the possible accuracy of the displacement estimation two signals are generated with single peaks, having different sub-pixel locations. As above, Gaussian and Airy functions are either sampled or partwise integrated to derive the discrete signals. From the maximum peak of the cross correlation function the sub-pixel location of the peak is derived using the model-based method described above.

Figure 12 shows the results for sampled Gaussian function for a peak width of

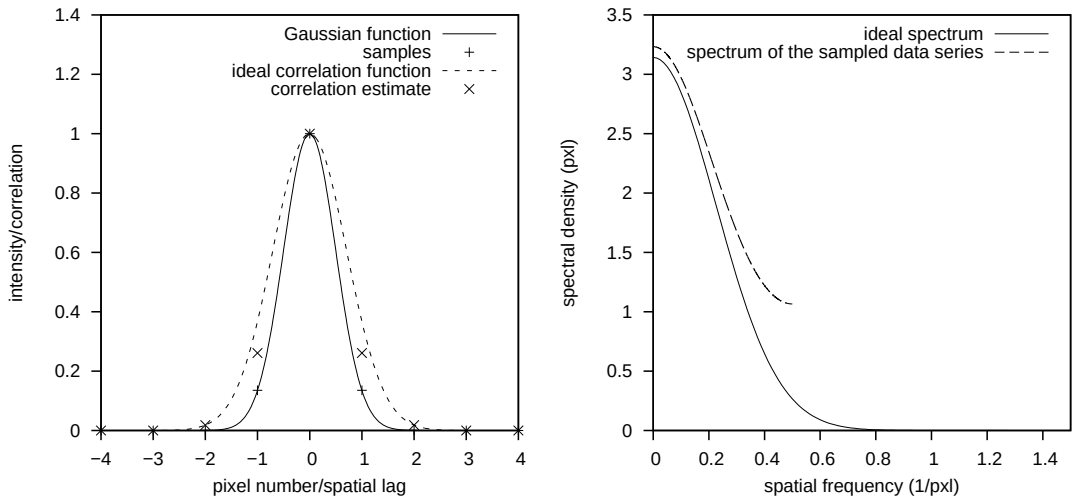

Figure 13: Deviation of the correlation estimate and the power spectral density function of the sampled series from the ideal Gaussian function

2.5 pxl. Even for this ideal case (single peak in each signal, sampled Gaussian function) a significant deviation can be seen between the estimated sub-pixel displacement and the simulation.

The cause of this phenomenon can be seen in figure 13. The continuous Gaussian function is sampled at discrete locations. Here the samples must fit the continuous function. Beside this, the autocorrelation function of the Gaussian function and the autocorrelation function of the sampled signal are shown. The autocorrelation function of the continuous Gaussian function is also a Gaussian function. A sub-pixel location of a Gaussian correlation function could be accurately estimated by the model-based method. However, the discrete correlation function of the sampled function does not fit in the continuous correlation function. Furthermore, even the shape is not Gaussian. The continuous Gaussian function has significant power in the frequency range above half the sampling frequency. Therefore, the Nyquist criterion is not fulfilled. Therefore, a significant aliasing error can be seen and a bias remains in sub-pixel estimation from the sampled correlation function even for a Gaussian signal.

In figure 14 the remaining bias of the sub-pixel displacement estimation from the correlation function is shown for several signals. Obviously, the systematic errors decrease for larger peak widths, independent of the signal shape. Two aspects are remarkable:

- The results for the partwise integrated functions are better than for the sampled functions. The integration causes a smoothing of the signal and the correlation function is more Gaussian-like.

- For peak widths up to 4 pxl, especially between 2.8 pxl and 3.8 pxl the bias for the partwise integrated Airy function is smaller than for the Gaussian

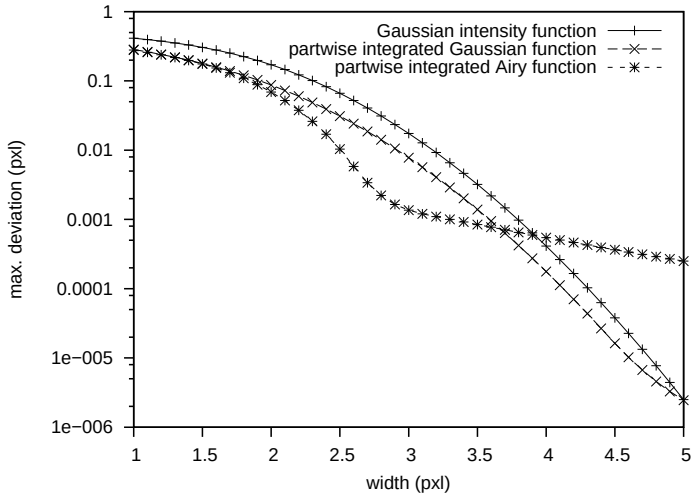

Figure 14: Sub-pixel displacement bias for the Gaussian model interpolation for several intensity functions

function. Obviously, the correlation function of the sampled Airy function is more Gaussian-like than for the sampled Gaussian function.

These results correspond to an image analysis without interpolation or window deformation, where the particles collectively move without any velocity gradient within the investigated area.

4.2 Estimation from single peaks with image interpolation

In this section the remaining estimation error of the sub-pixel displacement between two interpolated images is investigated. This corresponds e.g. to the image transform from image coordinates into real length coordinates or the correlation estimation from distorted images, which require a sub-pixel image interpolation. For simplification, again only one-dimensional signals are used.

Two signals are generated with single peaks, having different sub-pixel locations. As above, Gaussian and Airy functions are either sampled or partwise integrated to derive the discrete signals, which are interpolated to obtain a re-sampled signal. To isolate the bias caused by the interpolation scheme, a 4-times oversampling of the interpolated function is used. From the maximum peak of the cross-correlation function the sub-pixel location of the peak is derived using the model-based method described above.

The variation of the location of the peaks and the re-sampling positions in two signals and the variation of the peak width yields a 5-dimensional dependence of the remaining sub-pixel displacement bias. To reduce the number of variables, statistical averaging is used, quantified by the RMS value of the sub-pixel displacement bias.

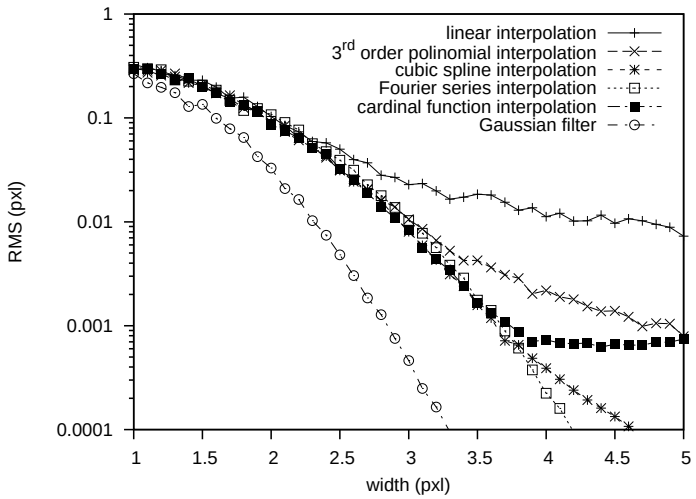

Figure 15: RMS value of the sub-pixel displacement error for Gaussian intensity functions for several interpolation methods

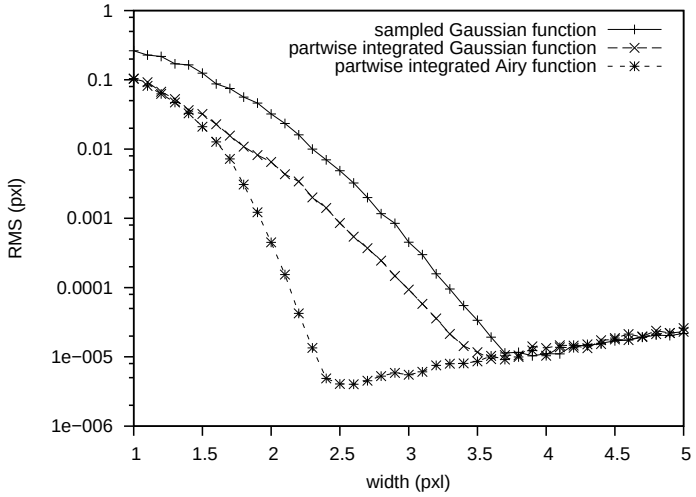

Figure 16: RMS value of the sub-pixel displacement error for the Gaussian model interpolation for several intensity functions

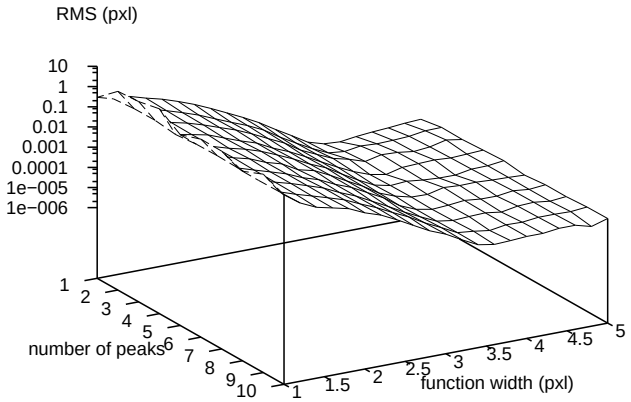

Figure 17: RMS value of the sub-pixel displacement error for the Gaussian model interpolation applied to a sampled Gaussian intensity function

Figures 15 and 16 show the RMS values of the sub-pixel displacement bias for the sampled Gaussian intensity function using different interpolation schemes and for the Gaussian filter interpolation for different intensity function respectively. The Gaussian filter interpolation is clearly superior. For a peak width of 2.3 pxl of the sampled Gaussian intensity function a sub-pixel displacement RMS value of 0.01 pxl remains. For the partwise integrated Gaussian function and the partwise integrated Airy function the RMS value is even smaller.

4.3 Estimation from multiple peak signals

To recognize the influence of multiple peaks, the investigation of the remaining RMS value of the sub-pixel displacement bias is performed also with multiple peak signals. The peaks have random location in the signal and random amplitudes, where all peaks have identical displacement between the two signals. Again the two signals are interpolated and re-sampled with a 4-times oversampling. The displacement between the two signals, the re-sampling positions and the peak widths are varied.

The RMS value of the sub-pixel displacement error is almost independent of the number of peaks in the signal. In figure 17 the results for the Gaussian model interpolation applied to a sampled Gaussian intensity function are shown. Similar results can be achieved for other intensity functions and other interpolation schemes.

Note that the situation changes, if no oversampling is used. In that case also the bias of the correlation peak interpolation, caused by the non-Gaussian shape of the sampled correlation function occurs. Furthermore, there is a dependence of the remaining bias on the number of peaks if no interpolation is used (figure 18).

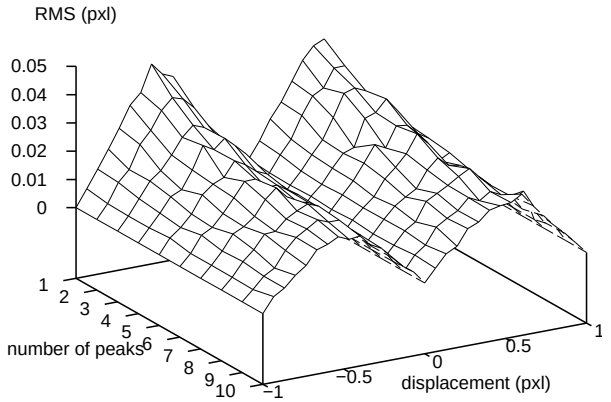

Figure 18: RMS value of the sub-pixel displacement error for the sampled Gaussian intensity function without interpolation

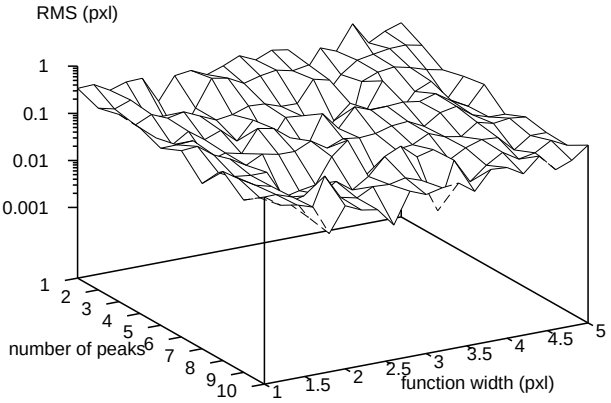

Figure 19: RMS value of the sub-pixel displacement error for the Gaussian model interpolation applied to a sampled Gaussian intensity function with edging influence

4.4 Peak Truncation

In the previous sections only signals with entire peaks have been used. The use of interrogation windows for PIV analysis yields a sharp sub-division of the image. Due to the random distribution of particles in the observed area, particle images can occur close to the edge of the interrogation window leading to truncated peaks.

In figure 19 the results for the Gaussian model interpolation applied to a sampled Gaussian intensity function are shown using an FFT based correlation estimator, which assumes a periodically continued function. For the two-dimensional case with the two intensity functions $z_1(i,j)$ and $z_2(i,j)$ this estimator can be written as

$$R(k,l) = \frac{1}{MN} \sum_{i=1}^{M} \sum_{j=1}^{N} z_1(i,j) z_2(i + k \mathrm{mod} M, j + l \mathrm{mod} M) \tag{5}$$

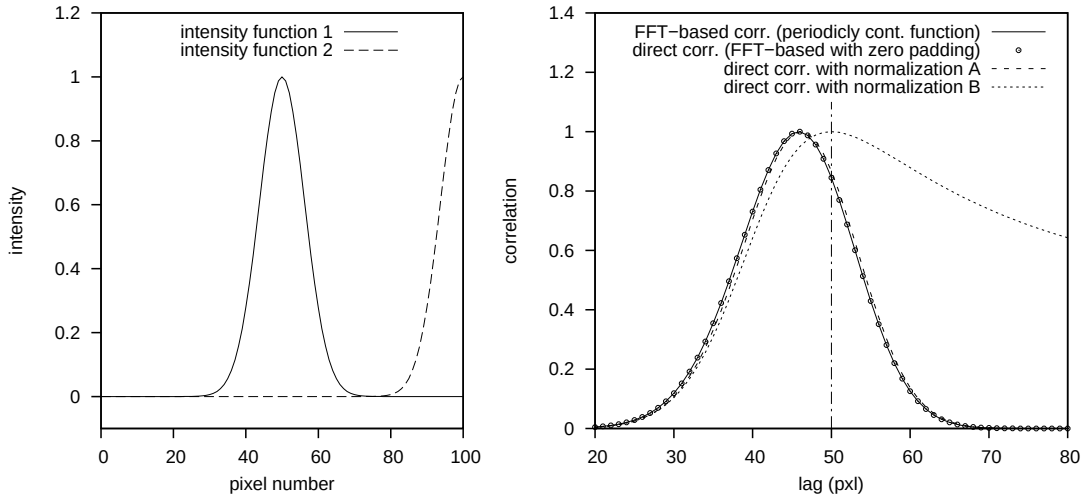

Figure 20: The truncation error of the correlation estimate

The RMS values are significantly higher than in figure 17, where only non-truncated peaks have been used.

This is due to a strong bias of the correlation maximum location in the case of truncated signals [Nogueira et al. (2001)]. Figure 20 shows the obtained correlation functions for a one-dimensional test case. The two intensity functions (figure 20a) have a displacement of 50 pixel, where the peak of the second signal is truncated. The maximum of the FFT-based correlation estimate is clearly shifted to lower values. Note, that all correlation estimates in figure 20b have been normalized to a maximum value of 1 for comparison.

Alternative correlation estimators, as the direct correlation estimate, without presumed periodicity

$$R(k,l) = \frac{1}{MN} \sum_{i=\max(1,1-k)}^{\min(M,M-k)} \sum_{j=\max(1,1-l)}^{\min(N,N-l)} z_1(i,j) z_2(i+k,j+l) \tag{6}$$

or the normalized direct correlation estimate (normalization A)

$$R(k,l) = \frac{1}{(M-|k|)(N-|l|)} \sum_{i=\max(1,1-k)}^{\min(M,M-k)} \sum_{j=\max(1,1-l)}^{\min(N,N-l)} z_1(i,j) z_2(i+k,j+l) \tag{7}$$

do not significantly improve the situation.

The influence of the truncation error can be escaped with the alternative normalization (B) using the variances of the two investigated image parts [Willert and Gharib (1991)], leading the correlation coefficient function

$$\rho(k,l) = \frac{\sum_{i=\max(1,1-k)}^{\min(M,M-k)} \sum_{j=\max(1,1-l)}^{\min(N,N-l)} z_1(i,j) z_2(i+k,j+l)}{\sqrt{AB}} \tag{8}$$

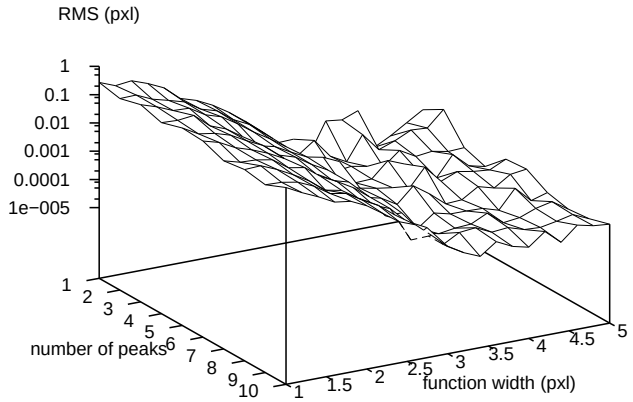

Figure 21: RMS value of the sub-pixel displacement error for the Gaussian model interpolation applied to a sampled Gaussian intensity function using the correlation coefficient estimation with normalization

with

$$A = \sum_{i=\max(1,1-k)}^{\min(M,M-k)} \sum_{j=\max(1,1-l)}^{\min(N,N-l)} z_1^2(i,j) \tag{9}$$

$$B = \sum_{i=\max(1,1-k)}^{\min(M,M-k)} \sum_{j=\max(1,1-l)}^{\min(N,N-l)} z_2^2(i+k,j+l) \tag{10}$$

Even for truncated peaks this estimator yields the correct location of the maximum and significant smaller RMS values of the sub-pixel displacement estimation bias (figure 21).

Note that also iterative displacement estimators with a window shift corresponding to the pre-estimated displacement [Westerweel et al. (1997)] reduce the influence of truncated peaks, since these estimators try to find and correlate those parts of the images with identical contents.

Therefore, the following investigations of the displacement estimation use an additional iterative algorithm, which shifts the interrogation windows by $\pm\frac{1}{2}$ of the estimated velocity to derive a better estimate of the velocity. The number of iterations is not given. The iteration runs until the optimum is found. The calculation is stopped or rejected, if the algorithm diverges or the estimated displacement is larger than the size of the interrogation area.

4.5 Noisy signals

In the case of an additional noise component in the signal, the width of the Gaussian filter must be adapted. A wide filter function, corresponding to a small b in equation (4) yields a smoother peak in the correlation function, where the noise is suppressed. However, also the systematic part of the peak is smoothed. Therefore, the accuracy of the estimation of the maximum location decreases.

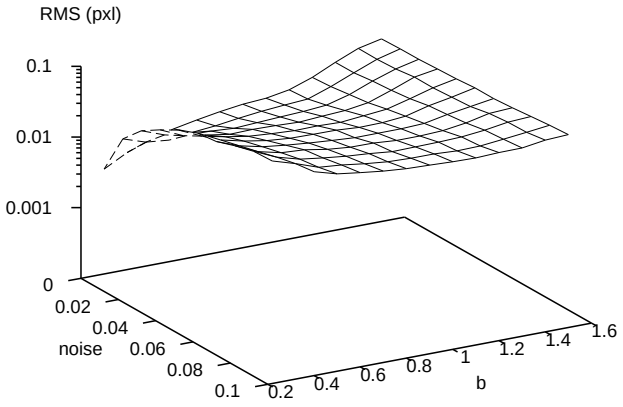

Figure 22: RMS value of the sub-pixel displacement error for the Gaussian model interpolation applied to a sampled Gaussian intensity function using the correlation coefficient estimation with normalization

Furthermore, in combination with an oversampling of the interpolated image, used to avoid the bias described in section 4.1, the correlation peak is wide and even small noise intensities yield a high probability of wrong displacement estimates.

To reduce the influence of the noise and to stabilize the displacement estimation, the correlation table can be downsampled, yielding smaller peaks. Note that the downsampling of the correlation table is not the inverse of the oversampling of the images. However, also the width of the Gaussian filter must be adapted. The filter parameter b in equation (4) must be set to about 0.5 for 1 % (noise amplitude/signal amplitude) and 1.1 for 10 % noise (figure 22).

5 Two-dimensional displacement estimation

The entire procedure of displacement estimation consists of

- image interpolation with over-sampling,
- correlation estimation,
- downsampling of the correlation table, and
- detection of the maximum location with sub-pixel estimation.

This procedure has the three parameters

- width of the Gaussian filter,
- over-sampling factor, and
- down-sampling factor.

Table 1: Simulation parameters

Particle image type	sampled Airy function
Particle image width	2.5 pxl
Particle image intensity	equally distributed from $[0 \ldots 1]$
Gray offset	0.05
Noise	equally distributed from $[0 \ldots 0.05]$
Interrogation area	$32\,\text{pxl} \times 32\,\text{pxl}$
Displacement	$[\Delta x; \Delta y] = [-1 \ldots 1\,\text{pxl}; -1 \ldots 1\,\text{pxl}]$
Number of particles	Poison distribution with a mean of 40

In a computer simulation a series of images has been generated with varied estimation parameters. The other simulation parameters are given in table 1. Figure 23 shows the obtained RMS values of the estimation error and figure 24 the obtained probability of spurious estimates.

For a higher over-sampling the remaining estimation error decreases, whereas the mathematical requirements increase strongly. For any over-sampling factor, the remaining estimation error is smallest for no down-sampling (down-sampling factor 1). On the other hand, this procedure yields a high probability of spurious estimates, so that a higher down-sampling factor must be chosen. A good compromise between the accuracy, the probability of spurious estimates and the computational costs is given by an over-sampling factor of 2 in combination with a down-sampling factor of 2 and a Gaussian filter parameter $b = 0.9$. Furthermore, this combination yields very reliable results with a very small probability of spurious estimates (no spurious estimates have been registered in the simulation).

6 Application to simulated and real images

6.1 Simulated data

To investigate the performance of the new PIV algorithm, PIV images with varying parameters have been simulated. The fixed parameters and the varied parameters with their range are given in table 2.

In that case the remaining RMS error of the displacement estimate must be drawn over 4 varying parameters. In figure 25 the parameter regions are marked, where the algorithms have an RMS error of less than 0.01 pxl. The new algorithm reaches this value in wide parameter ranges. Only for noise levels above 0.08 pxl and for small particle images in combination with a small number of particles the algorithm does not reach this value. The conventional PIV algorithm does not reach this value at all. Therefore, in figure 26 the parameter ranges have been marked, where the RMS error is less than 0.04 pxl. The new algorithm fulfils this requirement for all parameter choices. The conventional PIV algorithm reaches

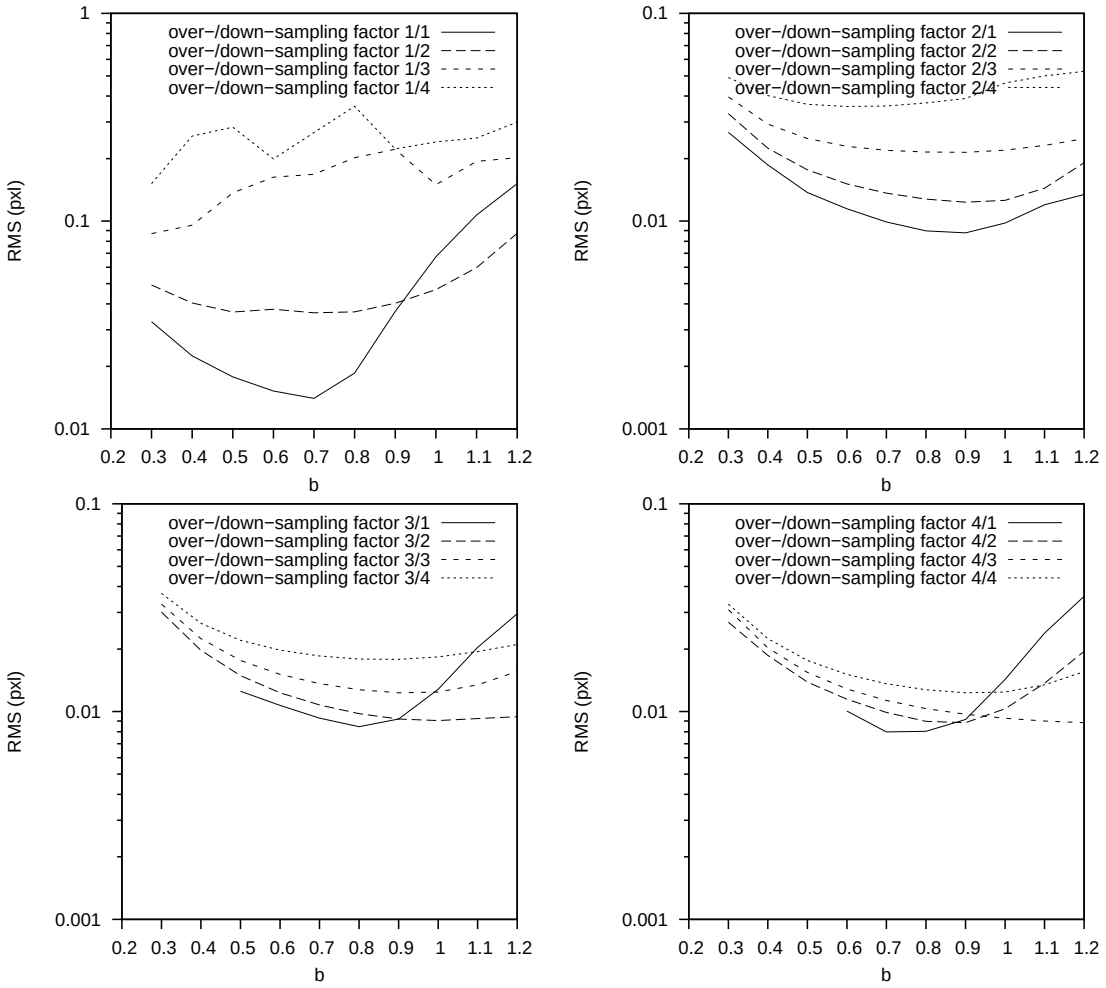

Figure 23: RMS value of the sub-pixel error for the two-dimensional displacement estimation

Table 2: Simulation parameters

Particle image type	sampled Airy function
Particle image width	$1.0 \ldots 5.5\,\mathrm{pxl}$
Particle image intensity	equally distributed from $[0 \ldots 1]$
Gray offset	$0.01 \ldots 0.09$
Noise	$0.01 \ldots 0.09$
Interrogation area	$32\,\mathrm{pxl} \times 32\,\mathrm{pxl}$
Displacement	$[\Delta x; \Delta y] = [-1 \ldots 1\,\mathrm{pxl}; -1 \ldots 1\,\mathrm{pxl}]$
Number of particles	$5 \ldots 55$

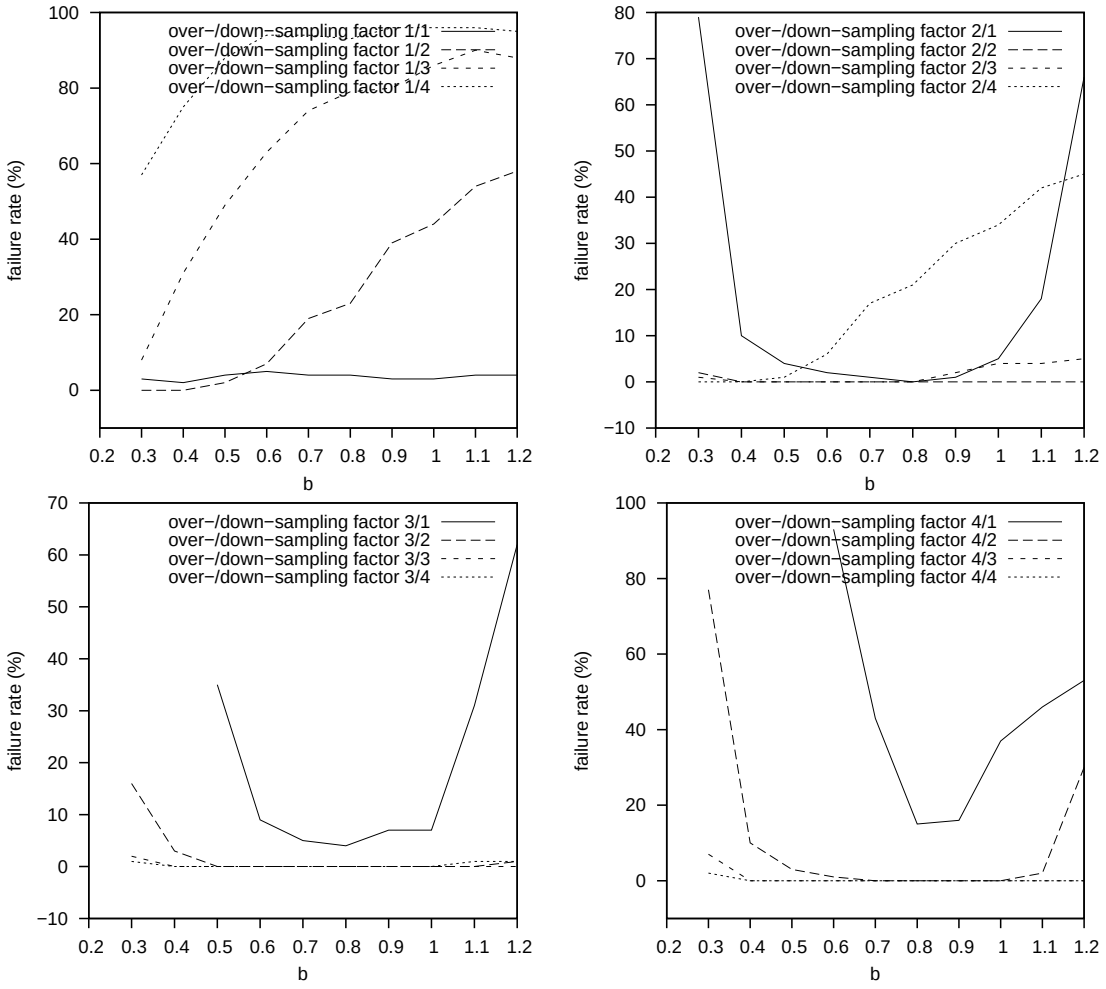

Figure 24: Failure probability of the sub-pixel error for the two-dimensional displacement estimation

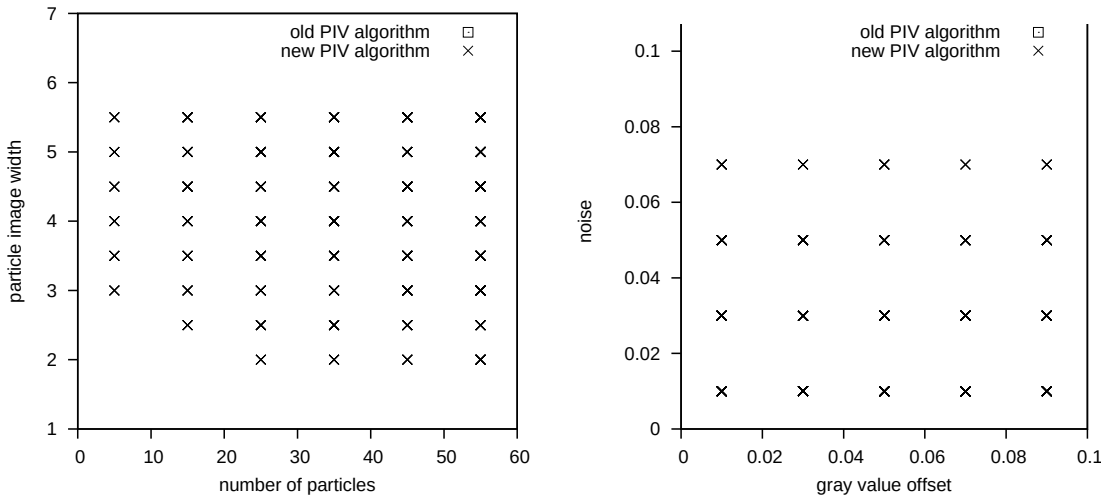

Figure 25: Paramater ranges with RMS errors less than 0.01 pxl

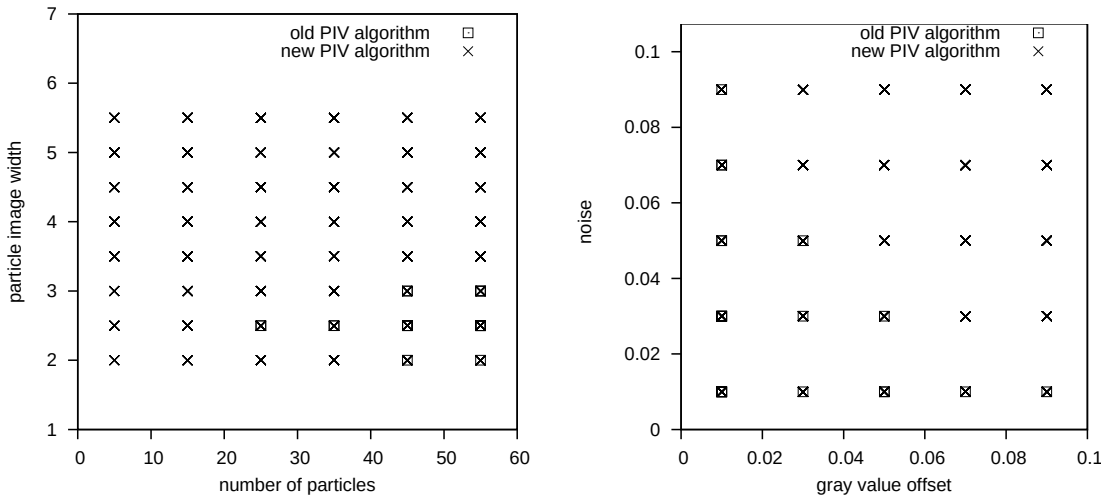

Figure 26: Paramater ranges with RMS errors less than 0.04 pxl

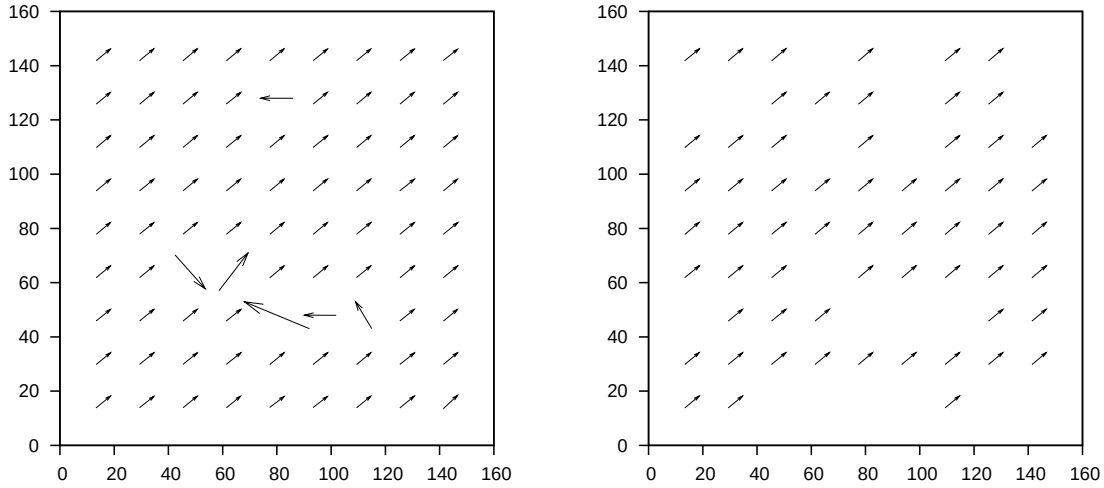

Figure 27: Results of the conventional (a) and the new (b) PIV algorithms applied to simulated image data

this limit only for particle image diameters between 2 and 3 pxl and only for a large number of particles in the measurement volume. On the other hand, the sum of the noise and the background gray level must be less than approximately 0.1.

The new algorithm clearly extends the application range of the PIV technique and, on the other hand, it yields more accurate velocity estimates. In figure 27 the images from figure 1 have been analyse with the common and the new PIV algorithm. The comparison clearly shows that the new algorithm yields more reliable results due to a significant reduction of spurious vectors.

6.2 Real data

To test the reliability of the new method, a real image pair (figure 28) has been taken from an experiment [Brede et al. (2003); Westergaard et al. (2003)]. The results of the new algorithm shown in figure 29 are more reliable than those of the conventional algorithm, which yields more spurious velocity vectors. Note that the flow field has spatial velocity gradients, hence due to the spatial averaging, the algorithm cannot reach the accuracy of the preceding sections and the sensitive validation often rejects the estimates.

7 Conclusions and Outlook

The improved PIV algorithm yields an accuracy of better than 0.01 pxl in wide parameter ranges for flow fields without velocity gradient. In the case of velocity gradients an averaging occurs, which limits the reachable accuracy. Therefore,

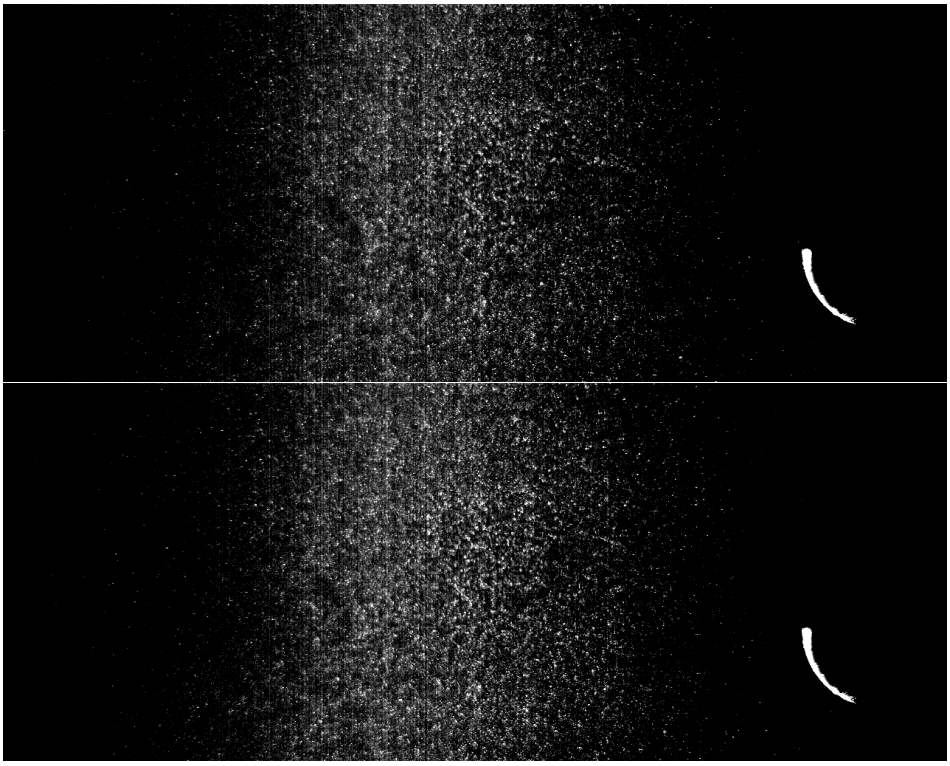

Figure 28: Experimental images

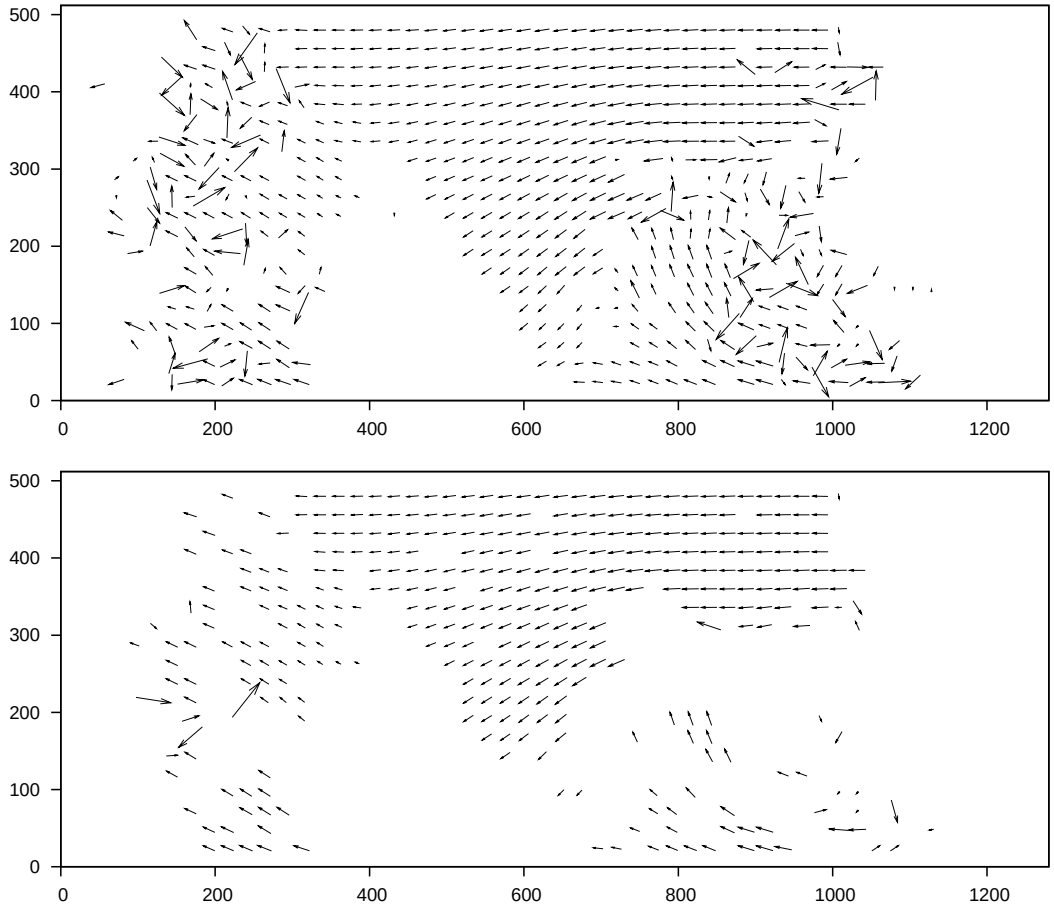

Figure 29: Results of the conventional (a) and the new (b) PIV algorithms applied to real image data

significant improvements can be achieved only with algorithms, which recognize or even estimate the velocity gradient. Furthermore, this technique can be combined with a model-based estimation of the flow field recognizing also the continuity of the flow.

References

Brede M, Leder A, and Westergaard CH (2003) Time-resolved piv investigation of the separated shear layer in the transitional cylinder wake. In Proc. 5th Int. Symp. on Particle Image Velocimetry. Busan, Korea. Paper 3215

Hall EL (1979) Computer Image Processing and Recognition. New York: Academic

Huang HT, Fiedler HE, and Wang JJ (1993) Limitation and improvement of piv; part ii: Particle image distorsion, a novel technique. *Exp. in Fluids* 15: 263–273

Niblack W (1986) An Introduction to Digital Image Processing. Englewood Cliffs, NJ: Prentice-Hall

Nogueira J, Lecuona A, and Rodriguez PA (2001) New source of peak locking to the window size: analysis and its removal. In Proc. 4rd Int. Workshop on PIV '01. Göttingen, Germany. Paper 1013

Pratt WK (1978) Digital image Processing. New York: Wiley

Roesgen T (2003) Optimal subpixel interpolation in particle image velocimetry. *Exp. in Fluids* 35: 252–256

Ronneberger O, Raffel M, and Kompenhans J (1998) Advanced evaluation algorithms for standard and dual plane particle image velocimetry. In Proc. 9th Int. Symp. on Appl. of Laser Techn. to Fluid Mechanics. Lisbon, Portugal. Paper 10.1

Scarano F (2002) Iterative image deformation methods in piv. *Meas. Sci. Technol.* 13: R1–R19

Westergaard CH, Brede M, Leder A, and Madsen BB (2003) Time-space analysis of time resolved piv data. In Proc. 5th Int. Symp. on Particle Image Velocimetry. Busan, Korea. Paper 3214

Westerweel J, Dabiri D, and Gharib M (1997) The effect of discrete window offset on the accuracy of cross-correlation analysis of digital piv recordings. *Exp. in Fluids* 23: 20–28

Willert CE and Gharib M (1991) Digital particle image velocimetry. *Exp. in Fluids* 10: 181–193